

Article

# Mn<sub>3</sub>O<sub>4</sub> Octahedral Microparticles Prepared by Facile Dealloying Process as Efficient Sulfur Hosts for Lithium/Sulfur Batteries

Yan Zhao <sup>1</sup>, Yuan Tian <sup>1</sup>, Xiaomin Zhang <sup>1</sup>, Zhifeng Wang <sup>1,\*</sup> , Taizhe Tan <sup>2</sup>, Zhihong Chen <sup>3,\*</sup> and Yichao Wang <sup>4</sup> 

<sup>1</sup> School of Materials Science and Engineering, Research Institute for Energy Equipment Materials, Hebei University of Technology, Tianjin 300130, China; yanzhao1984@hebut.edu.cn (Y.Z.); tianyuanhebut@163.com (Y.T.); xmzhang1223@163.com (X.Z.)

<sup>2</sup> Synergy Innovation Institute of GDUT, Heyuan 517000, China; taizhetan@gdut.edu.cn

<sup>3</sup> Shenyang Institute of Automation, Chinese Academy of Sciences, Guangzhou 511458, China

<sup>4</sup> School of Life and Environmental Sciences, Deakin University, Waurn Ponds, VIC 3216, Australia; yichaowang@gmail.com

\* Correspondence: zfwangmail@163.com (Z.W.); chenzhihong1227@sina.com (Z.C.)

Received: 30 May 2018; Accepted: 3 July 2018; Published: 4 July 2018



**Abstract:** A facile and industry-accepted dealloying method was used to synthesize Mn<sub>3</sub>O<sub>4</sub> particles, which were then employed to prepare sulfur/Mn<sub>3</sub>O<sub>4</sub> (S/Mn<sub>3</sub>O<sub>4</sub>) composites as cathode materials for lithium-sulfur batteries. The composites delivered initial discharge capacity reaching up to 1184 mAh·g<sup>-1</sup> at 0.1 C with capacity retention of 679 mAh·g<sup>-1</sup> after 150 cycles. In addition, even at 2 C, the lithium/sulfur battery with S/Mn<sub>3</sub>O<sub>4</sub> cathode delivered high reversible discharge capacity of 540 mAh g<sup>-1</sup>, demonstrating excellent rate capability.

**Keywords:** dealloying; Mn<sub>3</sub>O<sub>4</sub>; microparticles; lithium/sulfur batteries

## 1. Introduction

Rechargeable lithium-ion batteries (LIBs) have gained increasing attention during the past decades as they become widely used as promising power sources in portable electronic devices including cameras, laptops and mobile phones. However, the requirements in terms of specific capacity and rate capability of hybrid electric vehicles, power tools and the power grid must be enhanced [1,2]. Due to their high theoretical capacity of 1672 mAh·g<sup>-1</sup> and superior theoretical energy density of 2600 Wh·kg<sup>-1</sup>, lithium/sulfur (Li/S) batteries become one of the most promising candidates in LIBs [3]. Moreover, sulfur is non-toxic, naturally abundant, low-cost and environmentally friendly [4]. However, despite the advantages of Li/S batteries, several issues still require solutions for better practical applications [5]. In particular, their low conductivities limit the electron transport in the cathode and leads to low active material utilization. Also, the volume expansion (up to 80%) of S to Li<sub>2</sub>S leads to pulverization and collapse. Hence, the resulting soluble intermediate products lithium polysulfide (Li<sub>2</sub>S<sub>n</sub>, 4 < n < 8) contribute to low coulombic efficiency and active material loss [6,7]. Many means have been attempted to solve these problems, such as introduction of conductive carbon materials like carbon nanotubes [8–10], carbon spheres [11] and graphene [12–14], in an effort to improve the electronic conductivity of sulfur and accommodate the volume expansion during charge/discharge processes due to their porous structures and large specific surface areas.

Recently, some studies have focused on using metal oxides as additives or complexes in sulfur cathodes instead of carbon materials. Examples include Al<sub>2</sub>O<sub>3</sub> [15], ZnO [16], Mg<sub>0.6</sub>Ni<sub>0.4</sub>O [17], TiO<sub>2</sub> [18] and La<sub>2</sub>O<sub>3</sub> [19]. These metal oxides may provide superior electrochemical performances to

carbon-sulfur cathode materials. In particular, they can improve the performance of Li/S batteries over cycling, such as capacity, cycle stability and rate capability. This is because metal oxides could act as adsorbents and catalysts in lithium polysulfides. On the other hand, MnO is a promising sulfur host material due to its good structural stability and strong chemical anchoring effect towards soluble lithium polysulfides, which can suppress the shuttle effect. In previous reports, MnO was synthesized by co-precipitation or template. These methods are generally complex and hard to control, thus increasing the cost of the final products and restrict their applications as green anode materials of LIBs. Recently, it is found that dealloying is a simple method to produce metal oxides, which attracts considerable interest. Wada's group [20] has prepared three-dimensional nanoporous silicon material by dealloying in metallic melt and applied on the LIBs. They also synthesized bulk nanoporous silicon by dealloying method for presenting high cyclability of LIBs [21]. Chen and Sieradzki examined the formation of bicontinuous nanostructures during dealloying of Li from Li-Sn alloys, which contributes to the development of both dealloying and LIBs fields [22]. The obvious advantages of dealloying in terms of simple processing, short time consumption and low-cost, renders the method conducive to industrialization [23,24].

In this work,  $\text{Mn}_3\text{O}_4$  microparticles with strong adsorption capabilities to soluble polysulfides and high sulfur loading (67 wt. %) were first synthesized. The sulfur microparticles were then anchored on  $\text{Mn}_3\text{O}_4$  microparticles matrix, as cathodes of Li/S batteries. The structures, compositions and electrochemical performances of the resulting composites were evaluated.

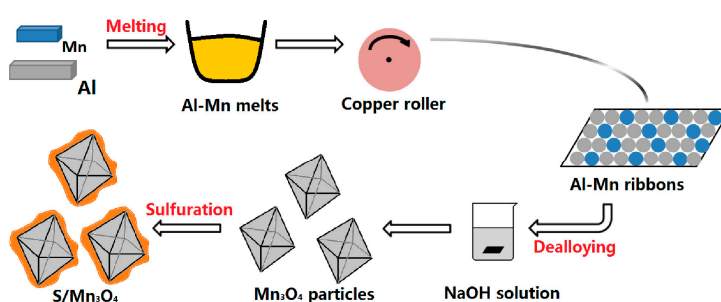
## 2. Materials and Methods

### 2.1. Preparation of $\text{Mn}_3\text{O}_4$ Microparticles

Firstly,  $\text{Al}_{95}\text{Mn}_5$  alloy melts (at. %) were obtained by melting pure Al (99.99 wt. %) and pure Mn (99.99 wt. %). The melts were then transferred to a holding furnace until gravity pouring the melts onto a single copper roller at rotating speed of 2000 r/min. This produced Al-Mn ribbons. Dealloying of the melt-spun Al-Mn ribbons was treated in 2 M NaOH aqueous solution with water bath at 25 °C for 36 h. After dealloying, the Al atoms were selectively dissolved. The residual Mn atoms carried out self-assembling and were oxidized into  $\text{Mn}_3\text{O}_4$  microparticles. The dealloying products were washed several times with deionized water and collected by centrifuge machine. The  $\text{Mn}_3\text{O}_4$  samples were finally obtained after drying for 24 h at 60 °C in vacuum drying chamber.

### 2.2. Preparation of S/ $\text{Mn}_3\text{O}_4$ Microparticles

The preparation of  $\text{Mn}_3\text{O}_4$  microparticles was typically carried out by mixing the  $\text{Mn}_3\text{O}_4$  and elemental sulfur at 1:3 mass ratio followed by grinding of the mixture for nearly 30 min to create a uniform powder. Next, the mixture was transferred into a stainless-steel autoclave and heated at 155 °C for 12 h. After cooling down to room temperature, the S/ $\text{Mn}_3\text{O}_4$  microparticles were obtained, with sulfur content estimated by chemical analysis to 67 wt. %. To better understand the fabrication process of this structure, the schematic representation is provided in Scheme 1.



**Scheme 1.** The schematic fabrication of S/ $\text{Mn}_3\text{O}_4$  microparticles.

### 2.3. Structural and Physical Characterization

The structures and phase compositions of the samples were determined by scanning electron microscopy (SEM, JSM-6700F, JEOL, Tokyo, Japan) at 1 nm and 15 kV, X-ray diffraction (XRD, D8 Discover, Bruker, Karlsruhe, Germany), transmission electron microscopy (HRTEM, JEM-2100F, JEOL, Tokyo, Japan) and X-ray photoelectron spectroscopy (XPS, Ulvac-Phi, Kanagawa, Japan).

### 2.4. Electrochemical Measurements

The S/Mn<sub>3</sub>O<sub>4</sub> electrodes were prepared by mixing 80 wt. % of the as-prepared S/Mn<sub>3</sub>O<sub>4</sub> microparticle powders, 10 wt. % polyvinylidene fluoride (PVDF, Kynar, HSV900, Colombes, France) as a binder and 10 wt. % Super-p as conducting agent in 1-methyl-2-pyrrolidinone (NMP, Sigma-Aldrich, St. Louis, MO, USA, 99.5% purity). The resultant slurry was then well-proportionally spread onto Al foils using a doctor blade and dried at 60 °C for 12 h.

The S/Mn<sub>3</sub>O<sub>4</sub> deposited films were used to prepare the electrodes through punching circular disks with 1.5 cm in diameter. The active material loading in each electrode was estimated to about 2 mg·cm<sup>-2</sup>. The coin cells were assembled in an Ar (99.9995%) filled MBraun glove box and tested galvanostatically on a multichannel battery tester (BT-2000, Arbin Instruments, College Station, TX, USA). The cut-off potential window was set to 1.5–3.0 V versus Li/Li<sup>+</sup> electrode and current densities were varied. All electrochemical measurements were performed at 25 °C.

## 3. Results and Discussion

The crystallographic structures of Mn<sub>3</sub>O<sub>4</sub> and S/Mn<sub>3</sub>O<sub>4</sub> microparticles were characterized by X-ray diffraction (XRD) spectroscopy and the results are shown in Figure 1. All main X-ray diffraction peaks appeared sharp, which can readily be assigned to Mn<sub>3</sub>O<sub>4</sub> phase (JCPDS No. 18-0838) and the other peaks are ascribed to sulfur, indicating the successful synthesis of S/Mn<sub>3</sub>O<sub>4</sub> [25].

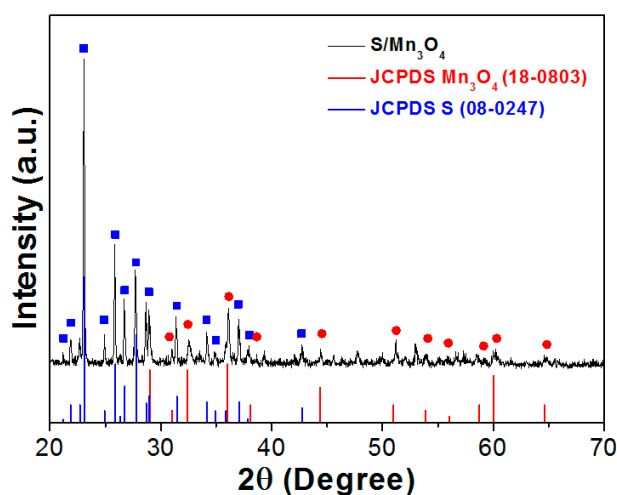


Figure 1. XRD patterns of S/Mn<sub>3</sub>O<sub>4</sub>.

The detected peaks of Mn 2p, O 1s and S 2p could be seen in the survey spectrum from XPS (Figure 2a), demonstrating the existence of Mn, O and S elements. The spectrum in Figure 2b presented two peaks of oxidized Mn at 641.6 eV and 653.5 eV, corresponding to Mn 2p<sub>3/2</sub> and Mn 2p<sub>1/2</sub>, respectively [26,27]. Figure 2c depicts the spectrum of O 1s, where two peaks attributed to bonds of OH coming from residual NaOH corrodent at 533.3 eV and Mn-O appeared at 531 eV, respectively. Figure 2d indicates a series of characteristic peaks at 162.5 eV, 164.4eV, 168.3 eV and 170.5 eV, consistent with S2p.

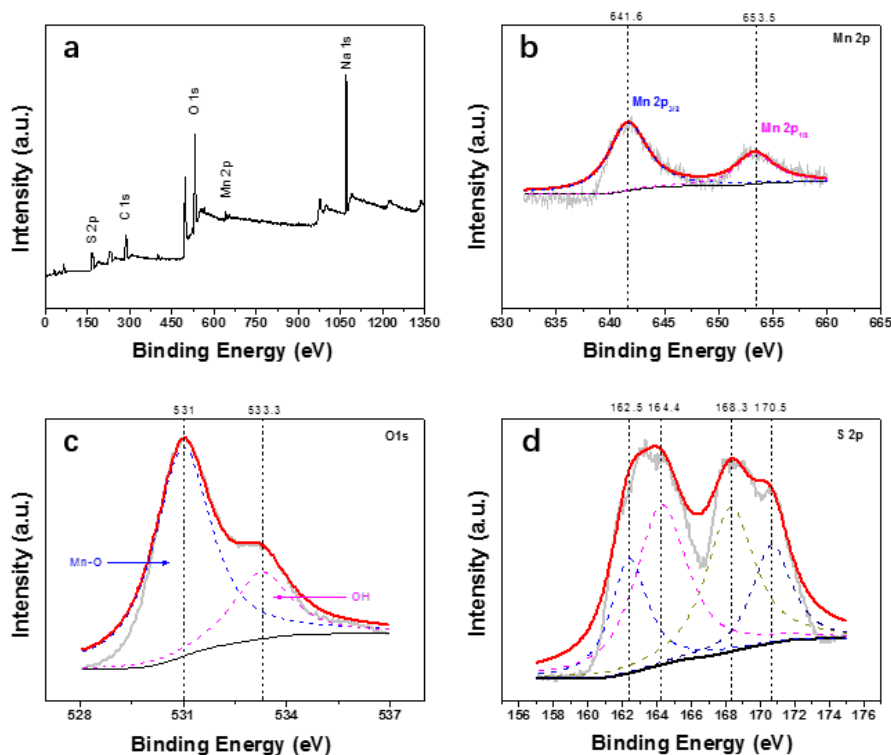


Figure 2. (a) The survey spectra of S/Mn<sub>3</sub>O<sub>4</sub>; (b) Mn 2p; (c) O 1s and (d) S 2p.

The SEM images of Mn<sub>3</sub>O<sub>4</sub> microparticles are illustrated in Figure 3. Octahedral microparticles with edge lengths of about 450 nm were homogeneously dispersed in Figure 3a. The surfaces of the octahedral microparticles looked highly faceted. The detailed structures of Mn<sub>3</sub>O<sub>4</sub> octahedral microparticles were further monitored by high magnification SEM imaging and the data are presented in Figure 3b.

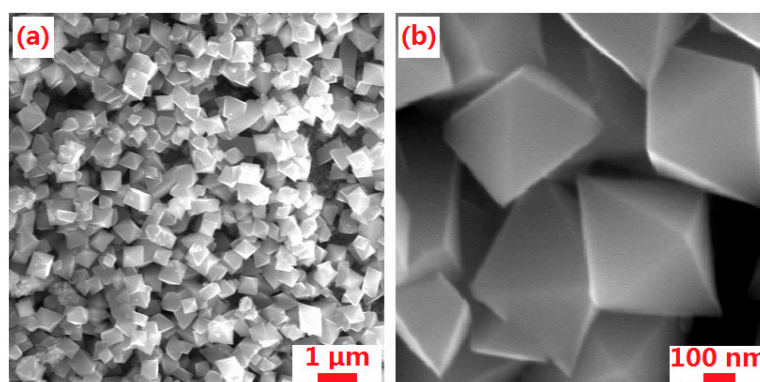
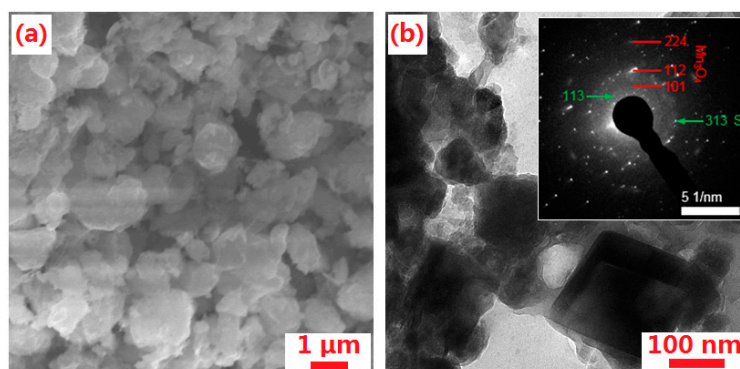


Figure 3. (a) SEM image and (b) high magnification SEM image of Mn<sub>3</sub>O<sub>4</sub> microparticles.

The morphology of S/Mn<sub>3</sub>O<sub>4</sub> is illustrated in Figure 4a. Numerous empty space left between particles could be observed, forming a 3D conductive structure. In-depth profiling of S/Mn<sub>3</sub>O<sub>4</sub> microparticle was further monitored by TEM imaging. As shown in Figure 4b, sulfur and Mn<sub>3</sub>O<sub>4</sub> microparticles were mixed uniformly. In the inset of Figure 4b, the corresponding selected area electron diffraction (SAED) pattern confirmed the polycrystalline diffraction ring of the sample corresponding to both Mn<sub>3</sub>O<sub>4</sub> and S phases. This also indicated that S/Mn<sub>3</sub>O<sub>4</sub> microparticle was successfully synthesized.



**Figure 4.** (a) SEM image and (b) high magnification TEM image and corresponding SAED patterns (inset) of S/Mn<sub>3</sub>O<sub>4</sub>.

The advantages of S/Mn<sub>3</sub>O<sub>4</sub> microparticle were demonstrated through the electrochemical performance evaluations of Li/S batteries, which were first tested by galvanostatic charge and discharge cycling. As presented in Figure 5, two main plateaus were visible in the initial discharge curves, corresponding to formation of high-order lithium polysulfides (Li<sub>2</sub>S<sub>n</sub>, 4 ≤ n ≤ 8) at 2.4 V, as well as further reduction to Li<sub>2</sub>S<sub>2</sub>/Li<sub>2</sub>S at 2.1 V [28]. The S/Mn<sub>3</sub>O<sub>4</sub> cathode exhibited elevated initial discharge capacity and maintained excellent reversible discharge capacity of about 1000 mAh·g<sup>-1</sup> after the 3rd cycle. No obvious change in the plateau position was detected in subsequent cycles, indicating the excellent cell reversibility and stability.

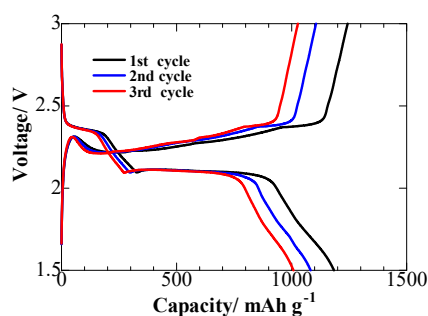


**Figure 5.** Charge and discharge curves of S/Mn<sub>3</sub>O<sub>4</sub> cathode.

The cells were then assembled to verify their cycling performances and rate capabilities (Figures 6 and 7). At 0.1 C, the cell presented an initial discharge capacity of about 1184 mAh·g<sup>-1</sup> and delivered a capacity of about 679 mAh·g<sup>-1</sup> after 150 cycles. The coulombic efficiency remained almost at 100% during the charge and discharge cycling, indicating the high stability of S/Mn<sub>3</sub>O<sub>4</sub> microparticle in the cathode and perfect control of the shuttle effect.

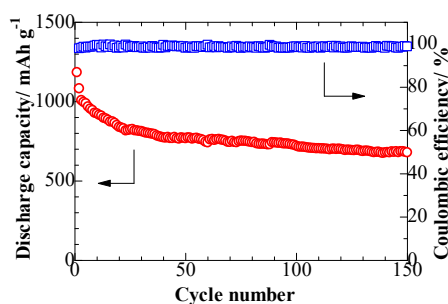


**Figure 6.** Cycling performance of S/Mn<sub>3</sub>O<sub>4</sub> cathode at 0.1 C.

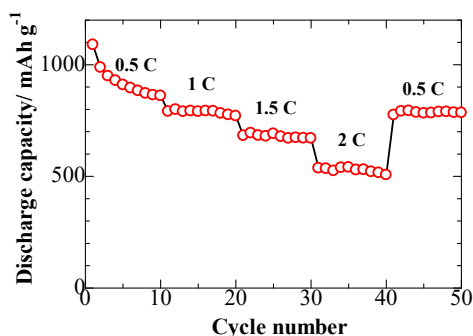


Figure 7. Rate performance of S/Mn<sub>3</sub>O<sub>4</sub> cathode.

As depicted in Figure 7, the cell subjected to various rates at 0.5 C, 1 C, 1.5 C and 2 C showed average discharge capacities of 930, 793, 683 and 540 mAh·g<sup>-1</sup>, respectively. After recovering to 0.5 C, the electrodes almost recovered the initial capacity of 789 mAh·g<sup>-1</sup>. This excellent rate performance of S/Mn<sub>3</sub>O<sub>4</sub> cathodes could be ascribed to the unique microparticle structures, which did not only provide pathways for electrolyte and Li-ion transport but also suppress the shuttle effect and enhanced the activity of the composite.

#### 4. Conclusions

Mn<sub>3</sub>O<sub>4</sub> octahedral microparticles were successfully synthesized by facile dealloying method. S/Mn<sub>3</sub>O<sub>4</sub> composites were then prepared by using the Mn<sub>3</sub>O<sub>4</sub> microparticles. When used as cathode materials for Li/S batteries, the S/Mn<sub>3</sub>O<sub>4</sub> composites exhibited high initial discharge capacities reaching up 1184 mAh·g<sup>-1</sup>. At cycling rates of 0.5 C, 1 C, 1.5 C and 2 C, the S/Mn<sub>3</sub>O<sub>4</sub> cathodes delivered high discharge capacities of 930, 793, 683 and 540 mAh g<sup>-1</sup>, respectively. After 150 cycles, the capacities of S/Mn<sub>3</sub>O<sub>4</sub> cathodes reached 679 mAh·g<sup>-1</sup>. These excellent electrochemical performances can be ascribed to structures of S/Mn<sub>3</sub>O<sub>4</sub> microparticles, which suppressed shuttle effect.

**Author Contributions:** Formal analysis, Y.Z., X.Z. and T.T.; Investigation, Y.T., X.Z.; Project administration, Z.W. and Y.Z.; Supervision, Z.W. and Z.C.; Writing-original draft, Y.Z. and Z.W.; Writing-review & editing, Y.W. and Z.C.

**Funding:** This work is financially supported by China Postdoctoral Science Foundation (2016M600190), Key Project of Science & Technology Research of Higher Education Institutions of Hebei Province, China (ZD2018059), Innovation & Entrepreneurship Training Program of Hebei University of Technology (201710080052), Guangdong Provincial Science and Technology Project (2017A050506009).

**Conflicts of Interest:** The authors declare no conflict of interest.

#### References

- Kang, B.; Ceder, G. Battery materials for ultrafast charging and discharging. *Nature* **2009**, *458*, 190–193. [[CrossRef](#)] [[PubMed](#)]
- Li, H.P.; Wei, Y.Q.; Zhang, Y.G.; Zhang, C.W.; Wang, G.K.; Zhao, Y.; Yin, F.X.; Bakenov, Z. In situ sol-gel synthesis of ultrafine ZnO nanocrystals anchored on graphene as anode material for lithium-ion batteries. *Ceram. Int.* **2016**, *42*, 12371–12377. [[CrossRef](#)]
- Kaiser, M.R.; Wang, J.; Liang, X.; Liu, H.K.; Dou, S.X. A systematic approach to high and stable discharge capacity for scaling up the lithium-sulfur battery. *J. Power Sources* **2015**, *279*, 231–237. [[CrossRef](#)]
- Zhang, Y.G.; Zhao, Y.; Konarov, A.; Li, Z.; Chen, P. Effect of mesoporous carbon microtube prepared by carbonizing the poplar catkin on sulfur cathode performance in Li/S batteries. *J. Alloy Compd.* **2015**, *619*, 298–302. [[CrossRef](#)]
- Manthiram, A.; Fu, Y.; Su, Y.S. Challenges and prospects of lithium-sulfur batteries. *Acc. Chem. Res.* **2013**, *46*, 1125–1134. [[CrossRef](#)] [[PubMed](#)]

6. Yin, F.X.; Liu, N.; Zhang, Y.G.; Zhao, Y.; Menbayeva, A.; Bakenov, Z.; Wang, X. Well-dispersed sulfur anchored on interconnected polypyrrole nanofiber network as high performance cathode for lithium-sulfur batteries. *Solid State Sci.* **2017**, *66*, 44–49. [[CrossRef](#)]
7. Zhang, Y.G.; Bakenov, Z.; Zhao, Y.; Konarov, A.; Doan, T.N.L.; Malik, M.; Paron, T.; Chen, P. One-step synthesis of branched sulfur/polypyrrole nanocomposite cathode for lithium rechargeable batteries. *J. Power Sources* **2012**, *208*, 1–8. [[CrossRef](#)]
8. Zhao, Y.; Yin, F.X.; Zhang, Y.G.; Zhang, C.W.; Mentbayeva, A.; Umirov, N.; Xie, H.X.; Bakenov, Z. A free-standing sulfur/nitrogen-doped carbon nanotube electrode for high-performance lithium/sulfur batteries. *Nanoscale Res. Lett.* **2015**, *10*, 1–6. [[CrossRef](#)] [[PubMed](#)]
9. Zhang, Y.G.; Zhao, Y.; Bakenov, Z.; Tuiyebayeva, M.; Konarov, A.; Chen, P. Synthesis of Hierarchical Porous Sulfur/ Polypyrrole/Multiwalled Carbon Nanotube Composite Cathode for Lithium Batteries. *Electrochim. Acta* **2014**, *143*, 49–55. [[CrossRef](#)]
10. Huang, J.Q.; Chong, W.G.; Zheng, Q.B.; Xu, Z.L.; Cui, J.; Yao, S.S.; Wang, C.W.; Kim, J.K. Understanding the roles of activated porous carbon nanotubes as sulfur support and separator coating for lithium-sulfur batteries. *Electrochim. Acta* **2018**, *268*, 1–9. [[CrossRef](#)]
11. Xiang, K.X.; Cai, S.Y.; Wang, X.Y.; Chen, M.F.; Jiang, S.X. Nitrogen-doped activated microporous carbon spheres as a sulfur matrix for advanced lithium-sulfur batteries. *J. Alloy Compd.* **2018**, *740*, 687–694. [[CrossRef](#)]
12. Tian, Y.; Sun, Z.H.; Zhang, Y.G.; Wang, X.; Bakenov, Z.; Yin, F.X. Micro-spherical sulfur/graphene oxide composite via spray drying for high performance lithium sulfur batteries. *Nanomaterials* **2018**, *8*, 50. [[CrossRef](#)] [[PubMed](#)]
13. Yu, M.P.; Li, R.; Wu, M.M.; Shi, G.Q. Graphene materials for lithium-sulfur batteries. *Adv. Energy Mater.* **2015**, *1*, 51–73. [[CrossRef](#)]
14. Zhou, L.; Zong, Y.; Liu, Z.L.; Yu, A.S. A polydopamine coating ultralight graphene matrix as a highly effective polysulfide absorbent for high-energy Li-S batteries. *Renew. Energy* **2016**, *96*, 333–340. [[CrossRef](#)]
15. Yermukhambetova, A.; Bakenov, Z.; Zhang, Y.G.; Darr, J.A.; Brett, D.J.L.; Shearing, P.R. Examining the effect of nanosized Mg<sub>0.6</sub>Ni<sub>0.4</sub>O and Al<sub>2</sub>O<sub>3</sub> additives on S/polyaniline cathodes for lithium sulphur batteries. *J. Electroanal. Chem.* **2016**, *780*, 407–415. [[CrossRef](#)]
16. Gu, X.X.; Tong, C.J.; Wen, B.; Liu, L.M.; Lai, C.; Zhang, S.Q. Ball-milling synthesis of ZnO@sulfur/carbon nanotubes and Ni(OH)<sub>2</sub>@sulfur/carbon nanotubes composites for high-performance lithium-sulfur batteries. *Electrochim. Acta* **2016**, *196*, 369–376. [[CrossRef](#)]
17. Zhang, Y.G.; Zhao, Y.; Yermukhambetova, A.; Bakenov, Z.; Chen, P. Ternary sulfur/polyacrylonitrile/Mg<sub>0.6</sub>Ni<sub>0.4</sub>O composite cathodes for high performance lithium/sulfur batteries. *J. Mater. Chem. A* **2013**, *1*, 295–301. [[CrossRef](#)]
18. Yao, J.; Mei, T.; Cui, Z.Q.; Yu, Z.H.; Xu, K.; Wang, X.B. Hollow carbon spheres with TiO<sub>2</sub> encapsulated sulfur and polysulfides for long-cycle lithium-sulfur batteries. *Chem. Eng. J.* **2017**, *330*, 644–650. [[CrossRef](#)]
19. Qian, X.Y.; Zhao, D.; Jin, L.; Shen, X.Q.; Yao, S.S.; Rao, D.W.; Zhou, Y.Y.; Xi, X.M. Hollow spherical lanthanum oxide coated separator for high electrochemical performance lithium-sulfur batteries. *Mater. Res. Bull.* **2017**, *94*, 104–112. [[CrossRef](#)]
20. Wada, T.; Yamada, J.; Kato, H. Preparation of three-dimensional nanoporous Si using dealloying by metallic melt and application as a lithium-ion rechargeable battery negative electrode. *J. Power Sources* **2016**, *306*, 8–16. [[CrossRef](#)]
21. Wada, T.; Ichitsubo, T.; Yubuta, K.; Segawa, H.; Yoshida, H.; Kato, H. Bulk-nanoporous-silicon negative electrode with extremely high cyclability for lithium-ion batteries prepared using a top-down process. *Nano Lett.* **2014**, *14*, 4505–4510. [[CrossRef](#)] [[PubMed](#)]
22. Chen, Q.; Sieradzki, K. Spontaneous evolution of bicontinuous nanostructures in dealloyed Li-based systems. *Nat. Mater.* **2013**, *12*, 1102–1106. [[CrossRef](#)] [[PubMed](#)]
23. Zhao, W.M.; Fei, P.Y.; Zhang, X.M.; Zhang, Y.G.; Qin, C.L.; Wang, Z.F. Porous TiO<sub>2</sub>/Fe<sub>2</sub>O<sub>3</sub> nanoplate composites prepared by de-alloying method for Li-ion batteries. *Mater. Lett.* **2018**, *211*, 254–257. [[CrossRef](#)]
24. Wang, Z.F.; Fei, P.Y.; Xiong, H.Q.; Qin, C.L.; Zhao, W.M.; Liu, X.Z. CoFe<sub>2</sub>O<sub>4</sub> nanoplates synthesized by dealloying method as high performance Li-ion battery anodes. *Electrochim. Acta* **2017**, *252*, 295–305. [[CrossRef](#)]

25. Liao, Q.Y.; Li, S.Y.; Cui, H.; Wang, C.X. Vertically-aligned graphene@Mn<sub>3</sub>O<sub>4</sub>nanosheets for a high-performance flexible all-solid-state symmetric supercapacitor. *J. Mater. Chem. A* **2016**, *4*, 8830–8836. [[CrossRef](#)]
26. Jin, W.; Han, X.J.; He, Y.Z.; Zhang, B.; Xu, P.; Du, Y.C. Galvanic replacement mediated synthesis of rGO-Mn<sub>3</sub>O<sub>4</sub>-Pt nanocomposites for oxygen reduction. *RSC Adv.* **2016**, *6*, 89124–89129. [[CrossRef](#)]
27. Jin, G.Z.; Xiao, X.X.; Li, S.; Zhao, K.M.; Wu, Y.Z.; Sun, D.; Wang, F. Strongly coupled graphene/Mn<sub>3</sub>O<sub>4</sub> composite with enhanced electrochemical performance for supercapacitor electrode. *Electrochim. Acta* **2015**, *178*, 689–698. [[CrossRef](#)]
28. Lin, T.Q.; Tang, Y.F.; Wang, Y.M.; Bi, H.; Liu, Z.Q. Scotch-tape-like exfoliation of graphite assisted with element sulfur and graphene-sulfur composites for high-performance lithium-sulfur batteries. *Energy Environ. Sci.* **2013**, *6*, 1283–1290. [[CrossRef](#)]



© 2018 by the authors. Licensee MDPI, Basel, Switzerland. This article is an open access article distributed under the terms and conditions of the Creative Commons Attribution (CC BY) license (<http://creativecommons.org/licenses/by/4.0/>).